Article:
Chadet, S, Allard, J, Brisson, L et al. (11 more authors) (2022) P2x4 receptor promotes mammary cancer progression by sustaining autophagy and associated mesenchymal transition. Oncogene, 41 (21). pp. 2920-2931. ISSN 0950-9232

https://doi.org/10.1038/s41388-022-02297-8

Title Page

P2X4 RECEPTOR PROMOTES MAMMARY CANCER PROGRESSION BY SUSTAINING AUTOPHAGY AND ASSOCIATED MESENCHYMAL TRANSITION

Stéphanie CHADET[1#], Jordan ALLARD[1], Lucie BRISSON[2], Osbaldo LOPEZ-CHARCAS[1], Roxane LEMOINE[1], Audrey HERAUD[1], Stéphanie LERONDEL[3], Roseline GUIBON[2], Gaëlle FROMONT[2], Alain LE PAPE[3], Denis ANGOULVANT[1], Lin-Hua JIANG[5,6], Ruth MURRELL-LAGNADO[4*] & Sébastien ROGER[1,7*]

[1]University of Tours, EA4245 Transplantation, Immunology, Inflammation, Tours, France
[2]Inserm UMR1069, Nutrition, Growth and Cancer, University of Tours, Tours, France
[3]CNRS UPS44 TAAM, Centre d'Imagerie du Petit animal, Orléans, France
[4]School of Life Sciences, University of Sussex, Brighton, UK
[5]School of Biomedical Sciences, University of Leeds, Leeds LS2 9JT, UK
[6]Sino-UK Joint Laboratory of Brain Function and Injury and Department of Physiology and Pathophysiology, Xinxiang Medical University, Xinxiang 453003, China
[7]Institut Universitaire de France, Paris, France

[*]These authors contributed equally to the work as senior authors

[#]Correspondence should be addressed to:
Dr. Stéphanie Chadet,
EA4245 Transplantation, Immunology, Inflammation,
10 Boulevard Tonnellé, 37032 Tours, France,
Tel: (+33) 2 47 36 63 26, Email: stephanie.chadet@univ-tours.fr

- Competing Interests

  The authors declare no competing financial interests

- Funding

  This work was supported by the "Ministère de la Recherche et des Technologies", the "Ligue Nationale Contre le Cancer – Interrégion Grand-Ouest" to SR, the Région Centre-Val de Loire (grant "CanalEx" to SR), the Institut National du Cancer (grant INCA_16110 "PURINO4EXO" to SR). S.R. was recipient of a prize "Prix Ruban Rose Avenir 2017" from the Charity "le Cancer du sein: parlons-en!". S.C. was recipient of a post-doctoral grant from the School of Life Science, University of Sussex (UK) and from the AURCIL Association in Tours (France).

Abstract

Metastatic progression is a major burden for breast cancer patients and is associated with the ability of cancer cells to overcome stressful conditions, such as nutrients deprivation and hypoxia, and to gain invasive properties. Autophagy and epithelial-to-mesenchymal transition are critical contributors to these processes. Here, we show that the P2X4 purinergic receptor is upregulated in breast cancer biopsies from patients and it is primarily localised in endolysosomes. We demonstrate that P2X4 enhanced invasion *in vitro*, as well as mammary tumour growth and metastasis *in vivo*. The pro-malignant role of P2X4 was mediated by the regulation of lysosome acidity, the promotion of autophagy and cell survival. Furthermore, the autophagic activity was associated with epithelial–to-mesenchymal transition (EMT), and this role of P2X4 was even more pronounced under metabolic challenges. Pharmacological and gene silencing of P2X4 inhibited both autophagy and EMT, whereas its rescue in knocked-down cells led to the restoration of the aggressive phenotype. Together, our results demonstrate a previously unappreciated role for P2X4 in regulating lysosomal functions and fate, promoting breast cancer progression and aggressiveness.

52 **Introduction**

53 During tumour development and progression, cancer cells acquire new abilities in order to overcome
54 stressful microenvironmental conditions and fulfil energy demands required by their high metabolism
55 (1–3). Cancer cells can use autophagy as a powerful strategy to survive under metabolic challenges such
56 as nutrient deprivation and reduced oxygen supply within the tumour microenvironment (4). This
57 stringent microenvironment also drives the expression of transcription factors responsible for the
58 epithelial-to-mesenchymal transition (EMT) program (5,6), another major process for tumour
59 progression. EMT has been correlated with cancer aggressiveness and metastatic potential, and is
60 generally associated with autophagy (7,8), while the link between the two processes is still elusive.

61 Lysosomes are intracellular acidic compartments that are essential for the catabolic clearance and
62 recycling of defective macromolecules or organelles, during autophagy and also following endocytosis
63 of extracellular materials (9,10). Lysosome properties are dramatically altered in cancer cells (11,12)
64 and these induce cellular functions that are involved in cancer progression. These include EMT (13), the
65 release of extracellular matrix degrading enzymes such as lysosomal cathepsins (14), cancer cell
66 invasion and metastases (15,16) and also the acquisition of resistance to anticancer treatments (17).
67 Nevertheless, relatively little is known about the key molecular determinants that modulate lysosome
68 function and fate in cancers, and their dependence on microenvironmental conditions.

69 The P2X4 receptor belongs to the family of transmembrane ionotropic P2X receptors. While it acts as
70 an ATP-gated non-selective cation channel, like other members of the family, P2X4 differs from the
71 other subtypes by its predominant localization in endosomal and lysosomal organelles of immune cells,
72 rather than to the plasma membrane (18). In this study, we show that the P2X4 receptor is significantly
73 overexpressed in human breast cancer samples compared to normal tissues. P2X4 is targeted to acidic
74 compartments of highly invasive mammary cancer cells and sustained invasion *in vitro* as well as
75 mammary tumour growth and metastatic progression in a syngeneic model of mammary cancer in
76 immunocompetent mice. We further investigated whether lysosomal P2X4 regulates breast cancer cell
77 properties to support aggressiveness. Importantly, P2X4 promoted the autophagic flux and associated
78 maintenance of a mesenchymal phenotype, primarily under metabolic challenges. Collectively, our

79 results provide compelling evidence supporting endolysosomal P2X4 as a critical protagonist driving

80 cancer progression.

81

82 **Materials and Methods**

83 **Agonists, antagonists and reagents** – Chloroquine and bafilomycin A1 were purchased from Sigma-
84 Aldrich (France). Caspase 3 Assay kit and staurosporine were from Abcam (France). 5-BDBD was
85 purchased from Tocris (Bio-Techne, France) and pepstatin A was from Enzo Life Sciences. LysoSensor
86 Yellow/blue-DND 160, Lysotracker Red DND-99 and Click-iT Plus EdU Flow Cytometry Assay Kit
87 were purchased from Invitrogen (France). ProSense 680 Fluorescent Imaging Agent was from
88 PerkinElmer. FlowCellect™ Autophagy LC3 Antibody-based Assay Kit was purchased from Merck
89 Millipore (France).

90 **Cells and cell culture** - Murine mammary cancer cell line 4T1 from the Balb/cJ strain was purchased
91 from LGC Standards (France), and a stable 4T1-luc cell line expressing the luciferase gene (thereafter
92 called "4T1 cells") was obtained by transduction of cells with lentiviral vectors containing the luciferase
93 gene and blasticidin resistance gene for selection (GIGA Viral Vectors, Belgium). Stable 4T1 cell lines
94 not expressing the *P2rx4* gene were obtained using the CRISPR/Cas9 technique by transfection with the
95 *P2RX4* Double Nickase Plasmid (Santa Cruz, France). Clonal selection was performed by FACS sorting.
96 Two clones have been kept for this study, called "Cr4#1" and "Cr4#2". A null-target Double Nickase
97 Plasmid was also used to transfect 4T1 cells and this led to the selection of a control cell line, thereafter
98 called "Crctl" cell line. Efficiency of the CRISPR-mediated knock-down was assessed by RT-qPCR and
99 western blotting, and stability of clones was followed for a minimal duration of 6 weeks. All the 4T1
100 cell lines were cultured in RPMI supplemented with 10% foetal calf serum (FSC). Cells were grown at
101 37°C in a humidified 5% CO_2 incubator. For hypoxic experiments, cells were cultured in a hypoxic
102 chamber (Invivo 200, Ruskinn Technology; 1% O_2, 5% CO_2, 94% N_2).

103 **Plasmid transfection** – Plasmid pcDNA3.1 encoding wild-type mouse P2rx4 was used for the rescue
104 experiments. Empty plasmid (pcDNA3.1) was used as a control. GFP-RFP-LC3 vector (addgene
105 #21074) was used to distinguish autophagosomes (yellow puncta) from autolysosomes (red puncta).
106 Plasmid transfection was carried out using Opti-MEM (Gibco) and TransIT-X2 (Mirus), according to
107 the manufacturer's protocol.

108 **RNA extraction, reverse transcription and quantitative polymerase chain reaction (qPCR) –** Total
109 RNA was extracted using NucleoSpin® RNA kit (Macherey Nagel EURL, Germany), and reverse-
110 transcribed with the PrimeScript RT Reagent Kit (Ozyme, France). Quantitative PCR were performed
111 using SYBR qPCR Premix Ex Taq (Ozyme, France) and CFX CONNECT (Bio-rad, France). The
112 housekeeping gene was Tata-binding Protein (TBP).
113 The primers used were as follows:

Gene (mouse)	**Forward primers (5'→3')**	**Reverse primers (5'→3')**
P2rx4	CCTGGCTTACGTCATTGGGT	AAGTGTTGGTCACAGCCACA
Tbp	AAGGGAGAATCATGGACCAGAAC	GGTGTTCTGAATAGGCTGTGGAG
Cdh1	CAGTTCCGAGGTCTACACCTT	TGAATCGGGAGTCTTCCGAAAA
Zo1	GCCTCAGAAATCCAGCTTCTCGAA	GCAGCTAGCCAGTGTACAGTATAC
Snai1	CACACGCTGCCTTGTGTCT	GGTCAGCAAAAGCACGGTT
Twist	TTCTCGGTCTGGAGGATGGA	TCTCTGGAAACAATGACATCTAGG
Zeb1	ACCGCCGTCATTTATCCTGAG	CATCTGGTGTTCCGTTTTCATCA
Vim	ACCTCACTGCTGCCCTGCGT	CTCATCCTGCAGGCGGCCAA

114

115 **Western blotting** – Cells were washed twice with ice-cold PBS (Gibco), and then lysed with RIPA
116 Buffer including Protease Inhibitors (Roche Lifesciences). Protein concentration was measured using
117 Pierce® BCA Protein Assay Kit (Thermofisher Scientific, France) and 25 µg of total protein were
118 resolved on SDS-PAGE. Proteins were transferred onto nitrocellulose membrane, followed by western
119 blot analysis using indicated antibodies. Quantification of signal intensity was performed using ImageJ
120 software. Antibodies used for immunoblotting were as follows: P2X4 (Alomone, #APR-002, 1:300),
121 LC3B (Abcam, #ab51520, 1:3,000), p62 (Abcam, #ab109012, 1:30,000), E-cadherin (Santa Cruz, #sc-
122 7870, 1:1,000), vimentin (Cell signalling, #5741, 1:5,000), cathepsin D (Abcam, #ab6313, 1:1,000),
123 actin (Santa Cruz, #sc-47778, 1:1,000), and HSC-70 (Santa Cruz, #sc-7298, 1:5,000). For the analysis
124 of autophagic flux, densitometric analyses of the LC3-II bands were normalized to actin (LC3-II/actin).
125 Autophagic flux was then determined by division of the normalized value obtained in presence of
126 chloroquine (CQ+ conditions) by the normalized value obtained in absence of chloroquine (CQ-
127 conditions). Unprocessed original immunoblot scans are provided in Supplementary File.

128 **Lysosomal pH measurement** – Changes in lysosomal pH were detected using the LysoSensor
129 Yellow/Blue DND-160. 4T1 cells were treated with 3 µM LysoSensor for 10 minutes at 37 °C. Cells
130 were then washed twice, detached and resuspended in PBS. Before the first experiment, a spectrum scan
131 was performed using Hitachi F2700 spectrofluorimeter (Hitachi, Tokyo, Japan). Then, emission
132 fluorescences were measured by flow cytometry (BD FACS Melody Cell Sorter) with emission
133 wavelengths at 448 nm (BP 448/45 nm) and 500 nm (LP 500/50) with excitation at 405 nm. Lower
134 448/500 ratio indicates more acidic lysosomal pH. A total of 10,000 cell-gate events were acquired and
135 analysed per sample.

136 **Cell viability / proliferation –** Tetrazolium salt (MTT) assay was performed as previously described
137 (19). Briefly, cells were cultured for 1 to 5 days and cell viability was measured after incubation with
138 MTT during 60 minutes at 37°C. Resulting formazan crystals were dissolved in DMSO and the
139 absorbance was measured at 560 nm using a plate reader (Biotek EL800).

140 **Measurement of autophagy by flow cytometry – A**utophagic fluxes were carried out by flow
141 cytometry using the FlowCellect™ Autophagy LC3 Antibody-based Assay Kit (Merck Millipore,
142 CF200097) according to the manufacturer's instructions. Briefly, cells ($4x10^4$/well) were seeded in 96
143 well plate 24 hours before experiment. The day after, medium was replaced by fresh medium and cells
144 were either left untreated or treated for 6 hours with chloroquine (100 µM) or the lysosome inhibitor
145 Autophagy Reagent A (Merck Millipore, CS208212). Cells were subsequently permeabilized and
146 stained with anti-LC3/FITC. The median fluorescence intensity was measured by flow cytometry (BD
147 FACSCanto™ I flow cytometer (BD Biosciences).

148 **Caspase-3 activity –** 4T1 cells were cultured for 24 hours either in normoxic (CO_2 incubator, 21% O_2)
149 or hypoxic (hypoxic chamber, 1% O_2) conditions and either with or without staurosporine (1 µM) which
150 was added 6 hours before the end of the culture. Caspase-3 activity was subsequently assessed according
151 to the manufacturer's protocol (abcam, #ab39401). Absorbances were measured at 405 nm expressed
152 relative to the staurosporine condition, and normalized to the control (Crctl, 21% O_2). All experiments
153 were performed in duplicate.

154 **Invasion assays –** Cell invasiveness was measured as previously described (19) using 8-µm pore size
155 polyethylene terephthalate membrane inserts covered with Matrigel® matrix (Becton Dickinson,
156 France). Cells in the lower surface of the insert were stained with DAPI and nuclei were counted after
157 imaging with an Evos M7000 microscope (Thermofisher, France).

158 **Immunocytochemistry experiments** – Cells were grown for 24 hours on 18 mm coverslips in 21% or
159 1% O_2, with or without serum. For experiments using LysoTracker-Red DND-99 (Invitrogen, L7528),
160 cells were incubated with 100 nM LysoTracker for 1 hour. Cells were fixed in 4% paraformaldehyde
161 and then permeabilized with 0.1% Triton-X-100 for 15 minutes. Unspecific antibody binding was
162 blocked with 3% BSA for 20 minutes. Primary antibodies for P2X4 (Alomone, APR-002, 1:200), Lamp-
163 1 (Abcam, #ab25245, 1:800), LC3B (Abcam, #ab51520, 1:2000), p62 (Abcam, #ab109012, 1:400),
164 vimentin (Cell signalling, #5741, 1:100) or cathepsin D (Abcam, #ab6313, 1:200). were applied for 1.5
165 hours at room temperature or overnight at 4 °C. Cells were then extensively washed with PBS and
166 incubated with diluted Alexa Fluor 488- and/or Alexa Fluor 647-conjugated secondary antibodies for 1
167 hour. Coverslips were mounted on slides using ProLong® Gold Antifade Mountant with DAPI
168 (Invitrogen, France). Images were obtained using either a confocal fluorescence microscope (Leica SP8,
169 63x objective) or an epifluorescence microscope (EVOS M7000, 40x objective) and were analysed using
170 ImageJ software. LAMP-1 staining was used as a marker to determine lysosome abundance, size and
171 distribution using the particle measurement tool of the ImageJ software. Lysosome distance to the
172 plasma membrane was measured as the shortest distance to cell contour (manually drawn region of
173 interest in WGA-stained cells). The Pearson correlation coefficient for LC3/LAMP-1 co-localization
174 was determined with JACoP (20) for ImageJ software 1.53c.

175 **Clinical samples and immunohistochemistry –** The P2X4 protein expression in normal and tumoral
176 mammary tissues was analysed by immunohistochemistry. Normal breast and cancer biopsies from the
177 University-Hospital of Tours were from the tumour collection declared to the French Ministry of
178 Research (No. DC2008-308) and were prepared at the anatomopathology department of the University-
179 Hospital of Tours, France. Briefly, after deparaffinization and rehydration, sections were treated with a
180 high-pH (Tris buffer/EDTA, pH 9.0) target retrieval procedure (Dako PT-link; Dako, USA).

181 Endogenous peroxidase was then blocked by a commercial solution (Dako REAL), and incubated
182 overnight with a 1/200 dilution of the primary polyclonal rabbit anti-P2X4 antibody (APR-002;
183 Alomone) at 4 °C. Sections were then incubated with a commercial anti-rabbit-labelled polymer (Dako
184 EnVision FLEX; Dako) for 30 minutes at RT. Immunoreaction was finally revealed with 3-3′
185 diaminobenzidine solution (Dako) for 5 minutes. A positive reaction was identified by a cytoplasmic
186 dark-brown precipitate. To determine the protein expression in tissues, a qualitative scale was used, for
187 negative or low, medium and high expression.

188 Metastases and primary tumours from *in vivo* mouse experiments were fixed in formalin, included in
189 paraffin, and cut in 5 µm tissue sections. Slides were deparaffinized, rehydrated and heated in citrate
190 buffer pH6 for antigenic retrieval, prior to labelling with the anti-P2X4 antibody. Immunohistochemistry
191 was performed using the streptavidin-biotin-peroxidase method with diaminobenzidine as the
192 chromogen (Kit LSAB, Dakocytomation). Slides were finally counterstained with haematoxylin.
193 Negative controls were obtained after omission of the primary antibody or incubation with an irrelevant
194 antibody.

195 **Electron microscopy** – 4T1 cells were cultured for 24 hours in either 21% or 1% O_2 and then fixed for
196 24 hours in 4% paraformaldehyde, 1% glutaraldehyde (Sigma, St-Louis, MO) in 0.1 M phosphate buffer
197 (pH 7.2). Samples were washed in PBS and post-fixed by incubation with 2% osmium tetroxide (Agar
198 Scientific, Stansted, UK) for 1 hour. Cells were then fully dehydrated in a graded series of ethanol
199 solutions and propylene oxide. The impregnation step was performed with a mixture of (1:1) propylene
200 oxide/Epon resin (Sigma) and then left overnight in pure resin. Samples were then embedded in Epon
201 resin (Sigma), which was allowed to polymerize for 48 hours at 60°C. Ultra-thin sections (90 nm) of
202 these blocks were obtained with a Leica EM UC7 ultramicrotome (Wetzlar, Germany). Sections were
203 stained with 2% uranyl acetate (Agar Scientific), 5% lead citrate (Sigma) and observations were made
204 with a JEOL 1400 plus transmission electron microscope (JEOL, Tokyo, Japan).

205 ***In vivo* mammary cancer model –** All experiments have been approved by the Comité d'éthique du
206 Centre-Val de Loire and have been performed in accordance with the European Ethics rules (Ref

207 005377.01 Apafis #12960). All animals were bred and housed at the CNRS UPS44 – TAAM- CIPA
208 (CNRS Campus, Orléans, France), in controlled conditions with a 12-hour light/dark cycle at 22°C, and
209 free to food and water ad libitum. We developed a syngeneic and orthotopic mouse mammary cancer
210 model in female BALB/cJ immunocompetent mice. To do so, 4T1-luciferase-expressing mouse
211 mammary cancer cells were injected into the fifth mammary fat pad of 6 weeks-old mice. The luciferase
212 activity was used to follow tumour appearance and growth *in vivo*, following D-luciferin (150 mg/kg)
213 intraperitoneal injection and bioluminescent imaging (IVIS Lumina II, Perkin Elmer). Primary tumour
214 volume (mm^3) and growth over time were most effectively measured with a calliper, twice a week, and
215 calculated as ($L \times l^2$)/2 (in mm). Metastases were counted macroscopically at the completion of studies,
216 during autopsies. Animal weight was measured once a week. In the experiments, $1x10^4$ Crctl, Cr4#1 or
217 Cr4#2 4T1-derived mammary cancer-cells (see section "Cells and cell culture") in 100 µL of PBS
218 solution were injected in the mammary fat pad, under isoflurane inhalation, of wild-type BALB/cJ mice
219 (Janvier Labs, Saint Berthevin, France).
220 To evaluate cathepsin activity, ProSense 750 Fast (Perkin Elmer), which becomes fluorescently
221 activated when cleaved by cathepsins, was used. Mice received the fluorescent dyes within a single
222 intravenous injection (4 nmol in 100 µL PBS) once individual tumours reached 100 mm^3 size threshold.
223 Mice were imaged 24 and 48 hours post-injection using Ivis Lumina II imaging system (Perkin Elmer,
224 USA) and analysed with Living Image (4.4) software. *Ex vivo* imaging of tumours was also performed
225 after necropsy.

226 **Bioinformatic analyses** - Gene expression data were obtained from The Cancer Genome Atlas (TCGA)
227 and Genotype-Tissue Expression (GTEx) databases using the UCSC Xena Browser
228 (https://xenabrowser.net) (21). The IlluminaHiSeq (log2-normalized_count+1) files were downloaded
229 from the "TCGA Breast Cancer (TCGA-BRCA)" cohort, in order to compare expressions between
230 adjacent non-tumoral tissues and primary tumour. From the "TCGA TARGET GTEx" cohort, the
231 RSEM_norm_count (log2-normalized_count+1) files were downloaded, in order to compare
232 expressions between normal tissues, adjacent non-tumoral tissues, primary tumour and metastases. In
233 addition, Breast Cancer Gene-Expression Miner v4.5 (bc-GenExMiner v4.5) incorporating TCGA and

234 GTEX data (n=1,234) was used to confirm *P2RX4* expression in normal and tumoral tissues
235 (http://bcgenex.ico.unicancer.fr). P2X4 protein expression data were obtained from Clinical Proteomic
236 Tumor Analysis Consortium (CPTAC) and UALCAN interface
237 (http://ualcan.path.uab.edu/analysis.html) (22). For *P2RX4/CTSD* correlation, Pearson's rank rho
238 coefficient was calculated, and two-dimensional correlation scatter plot was obtained using the UCSC
239 Cancer Browser Interface.

240 **Statistics and reproducibility** - Data were displayed as mean ± s.e.m. or as median ± range where
241 indicated in the figure legends. For box plots, the upper and lower edges of the box indicate the first and
242 third quartiles (25th and 75th percentiles) of the data and the middle line indicates the median. Mann-
243 Whitney rank sum test, Wilcoxon matched-pairs signed rank test and two-tailed Student's t-tests were
244 used for comparisons between two groups. Kruskal-Wallis, One- or two-way ANOVAs were used for
245 comparisons of more than two groups, using GraphPad Prism v.9.0.0 (GraphPad Software). Confidence
246 intervals of 95% were used and significance was considered when the P value was less than 0.05. The
247 number of times an experiment was repeated is indicated in the figure legends.

248 **Results**

249 **Overexpression of P2X4 is associated with mammary tumour growth and metastatic progression.**
250 Purinergic receptors have recently emerged as central players in tumour development (23,24). Among
251 them, the ATP-gated P2X7 receptor has attracted specific attention (25,26), however not much is known
252 about the involvement of other P2X receptors. Therefore, we performed bioinformatics gene expression
253 analyses in breast cancer from The Cancer Genome Atlas (TCGA), using the UCSC Xena browser
254 (https://xenabrowser.net). Five out of the seven *P2RX* genes were deregulated at the transcript level in
255 primary tumours compared to adjacent non-tumoral breast tissues (Fig. 1A). *P2RX1, P2RX6* and *P2RX7*
256 were significantly down-regulated whereas *P2RX4* and *P2RX5* were up-regulated in breast tumours (Fig.
257 1A). For the latter two genes, *P2RX4* was more noticeably upregulated in breast cancer (median was
258 9.562) compared to adjacent non-tumoral tissue (median was 8.955), and this was independent of
259 tumoral grade (Supplementary Fig. S1A). *P2RX4* upregulation in primary breast tumours was confirmed
260 using bc-GenExMiner mining tool (Supplementary Fig. S1B). Moreover, *P2RX4* was upregulated in
261 multiple types of cancers (15/24 tested types of cancers; Supplementary Fig. S1C). It was also
262 overexpressed in metastases, as compared to both normal and adjacent non-tumoral tissues, but with a
263 similar expression level to that of primary tumours (Fig. 1B). The expression of P2X4 proteins was
264 assessed by immunohistochemistry on normal (10 tissues) and primary breast cancer tissues (108
265 tissues). No or weak staining was found in normal tissues, whereas 51% of breast cancer biopsies
266 exhibited P2X4 staining, which was mainly cytoplasmic with a granular aspect (Fig. 1C). The staining
267 was moderate in 32% and strong in 19% of breast tumour tissues (Fig. 1D). Overexpression of the P2X4
268 protein in breast tumours was confirmed using external data from Clinical Proteomic Tumor Analysis
269 Consortium (CPTAC) and UALCAN portal (Supplementary Fig. S1D).
270 In order to assess the potential role of P2X4 in mammary tumour growth, we developed an orthotopic
271 mammary cancer model in immunocompetent BALB/cJ mice implanted with 4T1 syngeneic murine
272 mammary cancer cells. From the parental 4T1 cell line stably expressing the luciferase gene (4T1-Luc),
273 we developed two cell lines with a permanent knockdown of *P2rx4*, named Cr4#1 and Cr4#2, and a
274 control cell line (Crctl). The efficiency of *P2rx4* knockdown was verified by RT-qPCR (Fig 1E) and

275 western blotting (Fig. 1F). P2X4 silencing reduced cell proliferation/survival, as assessed by MTT
276 reduction after 4 and 5 days of culture, compared to Crctl cells (Fig. 1G). EdU incorporation was also
277 reduced in Cr4#2 cells after 5 days of culture (Supplementary Fig. S1E).
278 Compared to Crctl, P2X4 knockdown in mammary cancer (Cr4) cells was associated with a significant
279 reduction of tumour growth, as assessed by bioluminescence imaging (BLI) (Fig. 1H and Supplementary
280 Fig. S1F) and calliper (Fig. 1I). Of note, the two Cr4 clones expressed higher levels of luciferase as
281 compared to Crctl cells (relative values were 1.00 for Crctl, 1.28 for Cr4#1 and 1.33 for Cr4#2), as
282 measured *in vitro*, suggesting that *in vivo* BLI results may slightly overestimate Cr4 cells colonization.
283 Nevertheless, mice injected with Cr4 cells showed a very weak BLI signal for metastases (no statistical
284 difference between Cr4#1 and Cr4#2), which did not increase over time (Fig. 1J). *Ex vivo* analyses
285 confirmed these results and revealed that mice bearing Cr4 cells did not develop any metastasis, while
286 Crctl bearing counterparts developed metastases, mainly in bones and lungs (Fig. 1K). *Ex vivo*
287 immunohistochemical analyses of primary tumours and metastases from Crctl injected mice showed a
288 significantly higher expression of P2X4 in metastases than in the primary tumour (Supplementary Fig.
289 S1G and H).
290
291 **P2X4 receptor is partially localised in endolysosomal acidic compartments and controls**
292 **autophagic flux.**
293 P2X4 has been found to be localized intracellularly in different cell types, predominantly within
294 endolysosomal compartments (27,28). Consistent with previous studies assessing P2X4 subcellular
295 distribution, P2X4 was predominantly expressed within intracellular puncta and demonstrated partial
296 co-localization with lysotracker, a marker of acidic compartments (Pearson's correlation coefficient
297 (PCC) = 0.49) in 4T1 cells (Fig. 2A). A similar distribution of P2X4 was observed in two highly invasive
298 human cancer cell lines, MDA-MB-231 and MDA-MB-435s (Supplementary Fig. S2A). Interestingly,
299 the knockdown of P2X4 in 4T1 cells was associated with an increase in the number of LAMP-1 positive
300 vesicles suggesting a perturbation in lysosome biogenesis (Fig. 2B and 2C). While there was no change
301 in lysosomes distance to the nucleus (Supplementary Fig. 2B), the lysosome distance to the cell surface
302 was higher in Cr4#2 cells (medians were 3.130 for Crctl and 4.128 μm for Cr4#2, Fig. 2D). No

303 difference was observed in lysosome average size (Fig. 2E). As lysosome accumulation may be
304 associated with defective autophagic lysosomal degradation (29,30), the expression of LC3-II and p62
305 proteins was measured under basal conditions and following treatment with chloroquine (CQ) to inhibit
306 autophagic degradation. The expression levels of both LC3-II (lower band) and p62 proteins were
307 increased in Cr4 cells compared with Crctl cells (Fig. 2F, left; Supplementary Fig. S2C). Autophagic
308 flux (ratio of LC3-II level w/o *vs.* with CQ) was significantly reduced in Cr4 cells (Fig. 2F, right). Flow
309 cytometry analyses of LC3 levels were in agreement with western blot results (Fig. 2G, left). Under
310 basal conditions, the fluorescence intensity of LC3-FITC in Cr4 cells was higher than in Crctl cells,
311 whereas the intensities were matched following CQ treatment. The median ratios of LC3-II MFI were
312 4.77, 3.44 and 3.30 in Crctl, Cr4#1 and Cr4#2, respectively (Fig. 2G, right). Similar results were
313 obtained using autophagic reagents from EMD Millipore's Autophagy LC3-antibody based kit
314 (Supplementary Fig. S2D). Immunolabelling of p62 showed a higher number of p62 puncta in Cr4 cells
315 (medians were 10.30 for Crctl and 18.83 for Cr4#2, Fig. 2H). Furthermore, the pharmacological
316 inhibition of P2X4 in the Crctl cells using the membrane-permeable antagonist 5-BDBD, significantly
317 increased the p62 expression (Supplementary Fig. S2E). Similarly, the measure of GFP/RFP
318 colocalization using RFP-GFP tandem fluorescent-tagged LC3 confirmed that the knock-down of P2X4
319 led to autophagosome accumulation (Figure 2I). In addition, following transient silencing of *P2RX4*
320 gene with siRNA (Supplementary Fig. S2F), the autophagic flux was reduced in human MDA-MB-435s
321 cancer cells, although this did not reach significance in the MDA-MB-231 cells (Supplementary Fig.
322 S2G and H). Rescue experiments confirmed that transfection of the wild-type mouse *P2rx4* gene in
323 Cr4#2 cells (Supplementary Fig. S2I) significantly reduced p62 level caused by P2X4 knock-down (Fig.
324 2J and K). The medians were 1.04 and 0.78 in empty vector- and P2X4-expressing Cr4#2 cells,
325 respectively (Fig. 2K, left). However, no significant differences were observed on the autophagic flux
326 in P2X4 rescued Cr4#2 cells. The medians were 2.73 and 3.07 in empty vector- and P2X4-expressing
327 Cr4#2 cells, respectively (Fig. 2K, right). Using RFP-GFP-LC3 reporter, we found that P2X4
328 overexpression decreased the number of yellow puncta, suggesting a restored autophagic process (Fig.
329 2L and Supplementary Fig. 2J).
330

331 **P2X4 receptor regulates autophagy and promotes cancer cell survival under metabolic challenges.**
332 During tumour development, cancer cells are subjected to considerable metabolic stresses such as
333 nutrient deprivation and hypoxia. Given the important role of autophagy in cancer cell survival within
334 a stressful microenvironment, we studied the effects of P2X4 on p62 abundance under hypoxic
335 conditions and with serum deprivation (Fig. 3A). The p62 protein level was upregulated in Cr4#2 cells
336 under serum starvation compared to control cells (Fig. 3B), suggesting an impairment of autophagic
337 flux. The same tendency was observed for LC3-II expression, which was non-significantly increased in
338 Cr4#2 cells (Supplementary Fig. S3). To further investigate whether P2X4 regulates the fusion of
339 lysosomes with autophagosomes under conditions of metabolic challenge, confocal images were taken
340 of Crctl and Cr4#2 cells, co-stained with anti-LC3 and anti-Lamp-1 antibodies (Fig. 3C). Serum
341 deprivation under both normoxic and hypoxic conditions, significantly increased the co-localization of
342 these two proteins in the Crctl cells (median increase, 1.38-fold in 21% O_2 and 1.82-fold in 1% O_2) but
343 not in the Cr4#2 cells (Fig. 3D). Together, these results suggest that formation of autolysosomes is
344 impaired by knockdown of P2X4. The autophagy defect was correlated with reduced number of
345 autolysosomes in the Cr4#2 cells observed by electron microscopy (Fig. 3E) and was associated with
346 increased apoptosis, as assessed by monitoring caspase-3 activity (Fig. 3F).
347
348 **P2X4 receptor regulates lysosomal exocytosis and invasive capacities.**
349 Lysosomal cathepsins have been shown to be related to cancer malignancy and poor patient prognosis
350 (14). Especially, the aspartyl protease cathepsin D, encoded by the *CTSD* gene, is correlated with breast
351 cancer aggressiveness (31). In 4T1 cells, cathepsin D partially colocalizes with P2X4 (PCC = 0.58) (Fig.
352 4A). At the transcript level, there is a significant correlation between *P2RX4* and *CTSD* expression in
353 human breast cancer tissues ($p < 0.001$, PCC = 0.334, Fig. 4B). Consistently with reported evidence,
354 *CTSD* is upregulated in breast primary tumour as well as in metastases compared to adjacent non-
355 tumoral tissues (Fig. 4C). The addition of the aspartate protease inhibitor pepstatin A decreased the
356 ability of the 4T1 cells to invade the extracellular matrix (Supplementary Fig. S4A). Functional activity
357 of extracellular cathepsins was measured using a fluorescent probe in the model of murine breast cancer,
358 and this demonstrated important activity in primary tumours (Fig. 4D), both *in vivo* and *ex vivo*. To

359 investigate whether P2X4 regulates lysosomal exocytosis, we studied the release of cathepsin D in
360 cancer cell supernatants. We found that the total amount of cathepsin D (both pro- and active forms) in
361 the extracellular space was significantly decreased in Cr4#2 cells compared to Crctl counterparts (Fig.
362 4E and F). No significant differences were observed in the intracellular contents (Fig. 4E and
363 Supplementary Fig. S4B), suggesting that maturation of lysosomal cathepsin D is not altered in Cr4#2
364 compared to Crctl cells. Consistently, the lysosomal pH of Cr4#2 cells was more acidic, as measured by
365 the shift in the ratio of fluorescence of the LysoSensor Yellow/Blue probe (Fig. 4G and H), supporting
366 that Cr4#2 cells are able to induce maturation of lysosomal enzymes. These data might suggest a reduced
367 ability of Cr4#2 cells to fuse lysosomes to the plasma membrane and to secrete intralysosomal
368 components. Silencing P2X4 in human cancer cells also reduced the levels of extracellular cathepsin D
369 (Supplementary Fig. S4C and D). Accordingly, the lack of P2rx4 expression caused a reduction of the
370 invasive potential of 4T1 cancer cells (Fig. 4I). The rescue of P2X4 in Cr4#2 cells led to a marked and
371 significant increase of cell invasiveness (2.98-fold, Fig. 4J). Consistent with these results, inhibiting
372 P2X4 using 5-BDBD reduced invasion of Crctl cells (Supplementary Fig. S4E). Silencing P2X4 also
373 significantly reduced invasiveness of MDA-MB-435s cells, while a tendency was observed in MDA-
374 MB-231 cells (Supplementary Fig. S4F and G). These data provide compelling support for the role of
375 P2X4 in lysosomal exocytosis and cancer cell invasiveness.
376
377 **P2X4 receptor drives mammary cancer cells towards a mesenchymal phenotype while improving**
378 **autophagy.**
379 Epithelial-to-mesenchymal transition (EMT) is typically associated with cell aggressiveness and
380 metastasis formation, involving extracellular matrix degradation by released proteases. We found that
381 P2X4 inhibition led to a transcriptional increase of Cdh1 (epithelial marker) and a decrease of Vim
382 (mesenchymal marker), especially in hypoxia, as assessed by RT-qPCR (Fig. 5A). The respective
383 protein expression of E-cadherin and vimentin was assessed by western blot (Fig. 5B). Hypoxia did not
384 significantly modify the level of E-cadherin but this was strongly upregulated when P2X4 was silenced
385 (1.88-fold in 21 % O_2 and 2.44-fold in 1 % O_2; Fig. 5C). Hypoxia increased the amount of vimentin in
386 Crctl cells (by 1.47). Silencing P2X4 led to a reduction of vimentin expression (by 62.4 % in 21 % O_2

387 and 56.6 % in 1 % O_2; Fig. 5C). The rescue of P2X4 in the knocked-down cells restored the
388 mesenchymal phenotype, as assessed by RT-qPCR (Fig. 5D) and western blot (Fig. 5E). While no
389 modification of E-cadherin expression was observed, P2X4 overexpression led to a significant increase
390 of vimentin (1.33-fold and 2.43-fold at mRNA and protein level, respectively; Fig. 5F). Studying the
391 architecture of vimentin intermediate filaments, we found that the organization of its network was
392 notably modified in Cr4#2 cells in which a weaker signal was observed as well as reduction of the
393 quantity of elongated fibres and its subcellular restriction to a perinuclear localization (Fig. 5G). The
394 analysis of another epithelial marker (Zo1) and mesenchymal transcription factors (Twist, Zeb1, Snai1)
395 by RT-qPCR confirmed the role of P2X4 in favouring mesenchymal phenotype (Fig. 5H). Silencing
396 P2X4 caused an increase of Zo1 and a decrease of EMT-related transcription factors Zeb1 and Twist, in
397 both normoxia and hypoxia conditions. Consistent with previous reports, hypoxia triggered upregulation
398 of mesenchymal genes in Crctl cells. Twist and Zeb1 upregulations were even stronger after five days
399 of culture in hypoxia (Supplementary Fig. S5A). Similar results were obtained in human MDA-MB-
400 435s (increase of CDH1 and ZO1; decrease of VIM and ZEB1) and MDA-MB-231 (increase of CDH1;
401 decrease of ZEB1 and SNAI1) cancer cells using siRNA targeting *P2RX4* gene expression
402 (Supplementary Fig. S5B and C). Interestingly, the autophagy inhibitor bafilomycin A1 led to the
403 significant reduction of Vim and Twist expressions without modifying the expression of Cdh1 (Fig 5I)
404 or the other markers (Supplementary Fig. S5D), suggesting that blocking the autophagy process impairs
405 EMT, and that P2X4 has a critical role in controlling these two related functions.
406

407 **Discussion**

408 A growing body of evidence indicates that the purinergic signalling plays multiple functions during
409 cancer development and progression. Here, we identified the elevated expression of P2X4 in human
410 breast cancer tissues compared to normal tissues, at both mRNA and protein levels. Our results show
411 that P2X4 is mainly distributed in the cytosolic compartment and partially localizes in acidic organelles
412 of breast cancer cells, as previously reported in different non-cancer cell types (28,32). The changes that
413 we have observed in autophagic flux and in lysosomes number, location and exocytosis suggest that
414 there is a reduction in lysosome fusion associated with the knockdown of P2X4 in 4T1 cancer cells.
415 These results are consistent with previous studies showing that endolysosomal P2X4 receptors can
416 mediate Ca^{2+} release from lysosomes to trigger lysosome fusion, P2X4 is orientated with its extracellular
417 domain facing the lumen and levels of ATP within the lumen are sufficiently high, that lysosome
418 alkalinization is sufficient to trigger P2X4 activation and lysosome fusion (33). The identification of
419 factors which promote lysosome alkalinization in cancer cells remains to be established. It has been
420 shown, however, that endolysosomes are heterogeneous and differ in their pH, and that their anterograde
421 trafficking to the cell surface is associated with alkalinization. Additionally, P2X7 has been shown to
422 be a regulator of lysosome pH, both in microglia and in retinal epithelial cells, and in normal rat kidney
423 (NRK) cells, activation of P2X7 receptors enhanced lysosomal P2X4 receptor activation (34).

424 We demonstrated that the inhibition of P2X4 in breast cancer cells led to a reduction of both autophagy
425 and lysosomal exocytosis, suggesting that P2X4 promotes fusion of lysosomes to either autophagosomes
426 or plasma membrane. Consistent with this hypothesis, it was previously observed that lysosomal P2X4
427 interacts with calmodulin for fusion of lysosomes with other compartments (18,33). Fusion with
428 autophagosomes is required for autophagy and, here, we found that P2X4 downregulation led to
429 autophagosome accumulation and an increase in caspase-3 activity. In particular, we observed the
430 accumulation of LC3-II in three highly invasive cancer cell lines when P2X4 was knocked-down, by
431 using either Crispr/Cas9 technology or siRNA. The role of P2X4 in autophagy was even more
432 pronounced under serum deprivation than in normal growth medium, as indicated by p62 expression. In
433 turn, overexpression of P2X4 in Cr4#2 cells resulted in a robust decrease of p62 and therefore the

434 restitution of autophagic activity. Supporting these results, a very recent study identifies P2X4 as a target
435 for indophagolin, an autophagy inhibitor, using thermal proteome profiling technology (35). In this
436 study, the reduced autophagic flux in Cr4#2 cells might partly be responsible for the inhibition of tumour
437 progression observed in our *in vivo* mammary cancer model. To overcome stressful conditions and fulfil
438 energy demands necessary for their metabolic functions, cancer cells may increase autophagy (3,36). In
439 this context, autophagy inhibition has been proposed as a treatment in a variety of cancers, including
440 breast cancer (37,38).

441

442 Depending on tumour stage, autophagy can trigger EMT. Typically, autophagy generates resistance to
443 cell death and several studies have shown that autophagy deregulation inhibits tumour growth and
444 metastatic spreading (39,40). By decreasing apoptosis and regulating the tumour microenvironment,
445 autophagy can support EMT, which is considered as a major process for cell invasiveness and metastasis
446 formation (8). One key finding of this study is to reveal that P2X4 has an important role in modulating
447 EMT. In all three cell lines, P2X4 inhibits the expression of epithelial markers E-cadherin and Zo-1,
448 while increasing the expression of mesenchymal genes. In 4T1 cells, the use of bafilomycin A1 led to
449 an inhibition of vimentin and Twist expressions, suggesting that autophagy inhibition may reduce the
450 expression of some EMT markers. Furthermore, P2X4 may also strengthen EMT by increasing
451 lysosome exocytosis and thereby influencing the tumour microenvironment (41,42), or by promoting
452 lysosome interaction with cytoskeleton-associated proteins, as previously observed (43,44). Indeed,
453 lysosomes interact with vimentin intermediate filaments and vimentin inhibition leads to juxtanuclear
454 lysosome accumulation and subsequent modulation of autophagy (45). In turn, lysosomal proteins can
455 modify the architecture of vimentin networks (46). Consistent with these observations, our results
456 indicate that P2X4 downregulation leads to an inhibition of vimentin expression and alteration of its
457 network. Conversely, the rescue of P2X4 restored high vimentin expression in P2X4 knocked-down
458 cells.

459 A range of studies have reported that vimentin regulates EMT through upregulation of EMT-associated
460 genes (47,48) and modifications of cell shape, motility, and adhesion (49). EMT is currently associated
461 with metastatic spreading, which require extracellular matrix degradation by extracellular proteases.
462 Here, we show a positive correlation between expression of *P2RX4* and *CTSD* in breast cancer.
463 Cathepsin D is reported to mediate tumour aggressiveness and expression of EMT genes and is
464 associated with poor patient prognosis (31,50). Consistent with studies showing the role of P2X4 in
465 lysosome fusion to the plasma membrane (18,51), our results suggest that P2X4 regulates the release of
466 the lysosomal cathepsin D in the extracellular compartment. Accordingly, P2X4 downregulation
467 compromises cell invasiveness, whilst its rescue restores this capacity.

468 In conclusion, our data reveal an important role of P2X4 in breast cancer cell functions, promoting
469 cancer cell invasiveness and resistance to metabolic challenges by regulating autophagy and lysosomal
470 exocytosis. As such, P2X4 may mediate hallmarks of cancer cell malignancy.

Data and materials availability

All data and materials used in this study are available upon request.

Acknowledgments

This work was supported by the "Ministère de la Recherche et des Technologies", the "Ligue Nationale Contre le Cancer – Interrégion Grand-Ouest" to SR, the Région Centre-Val de Loire (grant "CanalEx" to SR), the Institut National du Cancer (grant INCA_16110 "PURINO4EXO" to SR). S.R. was recipient of a prize "Prix Ruban Rose Avenir 2017" from the Charity "le Cancer du sein: parlons-en!". S.C. was recipient of a post-doctoral grant from the School of Life Science, University of Sussex (UK) and from the AURCIL Association in Tours (France).

We thank Mrs Carole Desplanches for secretary and administrative assistance. We thank Mrs Stéphanie Rétif, Mrs Marilyne Le Mée and M. Julien Sobilo for the assistance with *in vivo* experiments performed at CNRS UPS44 CIPA, Orléans. Our microscopy data were obtained with the assistance of the IBiSA Electron Microscopy Facility of the University of Tours, and we are grateful to M. Julien Burlaud-Gaillard for his help with electronic and confocal microscopy. We thank Dr Vinh Ta Phuoc for the insightful discussions on lysosomal distribution analyses.

Author contributions

All authors contributed extensively to the work presented in this study. S.C. performed cell culture, molecular and cellular biology experiments, assessed cell viability, apoptosis and invasion, immunofluorescence/confocal imaging, flow cytometry, pH imaging, bioinformatics and statistical analyses. J.A. performed invasion and molecular biology experiments. L.B. and R.L. participated in cell culture, flow cytometry and scientific input regarding autophagy analysis. A.H. and J.A participated to cell culture. O. L.-C., J.A. and L.-H.J. participated to rescue experiments. R.G. and G.F. performed IHC analyses. S.C., S.L. and A.L.P. performed *in vivo* mouse experiments. SC., R.M.-L. and S.R. analysed *in vivo* data. S.R. and R.M.-L. obtained research grants. D.A. and L.-H.J. participated to critical reading of the manuscript. S.C., S.R. and R.M.-L. directed the research, designed the study, analysed the data, and wrote the manuscript.

Competing Interests

The authors declare that they have no conflict of interest.

References

1. Mathew R, Karantza-Wadsworth V, White E. Role of autophagy in cancer. Nat Rev Cancer. 2007 Dec;7(12):961–7.

2. Gouirand V, Guillaumond F, Vasseur S. Influence of the Tumor Microenvironment on Cancer Cells Metabolic Reprogramming. Front Oncol [Internet]. 2018 [cited 2020 Oct 22];8. Available from: https://www.frontiersin.org/articles/10.3389/fonc.2018.00117/full

3. Kimmelman AC, White E. Autophagy and Tumor Metabolism. Cell Metab. 2017 May 2;25(5):1037–43.

4. Levine B. Autophagy and cancer. Nature. 2007 Apr;446(7137):745–7.

5. Martin FT, Dwyer RM, Kelly J, Khan S, Murphy JM, Curran C, et al. Potential role of mesenchymal stem cells (MSCs) in the breast tumour microenvironment: stimulation of epithelial to mesenchymal transition (EMT). Breast Cancer Res Treat. 2010 Nov 1;124(2):317–26.

6. Brabletz T, Kalluri R, Nieto MA, Weinberg RA. EMT in cancer. Nat Rev Cancer. 2018 Feb;18(2):128–34.

7. Gugnoni M, Sancisi V, Manzotti G, Gandolfi G, Ciarrocchi A. Autophagy and epithelial–mesenchymal transition: an intricate interplay in cancer. Cell Death Dis. 2016 Dec;7(12):e2520–e2520.

8. Chen H-T, Liu H, Mao M-J, Tan Y, Mo X-Q, Meng X-J, et al. Crosstalk between autophagy and epithelial-mesenchymal transition and its application in cancer therapy. Mol Cancer. 2019 May 24;18(1):101.

9. Saftig P, Klumperman J. Lysosome biogenesis and lysosomal membrane proteins: trafficking meets function. Nat Rev Mol Cell Biol. 2009 Sep;10(9):623–35.

10. Lahiri V, Hawkins WD, Klionsky DJ. Watch What You (Self-) Eat: Autophagic Mechanisms that Modulate Metabolism. Cell Metab. 2019 Apr 2;29(4):803–26.

11. Hämälistö S, Jäättelä M. Lysosomes in cancer—living on the edge (of the cell). Curr Opin Cell Biol. 2016 Apr 1;39:69–76.

12. Kallunki T, Olsen OD, Jäättelä M. Cancer-associated lysosomal changes: friends or foes? Oncogene. 2013 Apr;32(16):1995–2004.

13. Janda E, Nevolo M, Lehmann K, Downward J, Beug H, Grieco M. Raf plus TGF β -dependent EMT is initiated by endocytosis and lysosomal degradation of E-cadherin. Oncogene. 2006 Nov;25(54):7117–30.

14. Olson OC, Joyce JA. Cysteine cathepsin proteases: regulators of cancer progression and therapeutic response. Nat Rev Cancer. 2015 Dec;15(12):712–29.

15. Brix DM, Tvingsholm SA, Hansen MB, Clemmensen KB, Ohman T, Siino V, et al. Release of transcriptional repression via ErbB2-induced, SUMO-directed phosphorylation of myeloid zinc finger-1 serine 27 activates lysosome redistribution and invasion. Oncogene. 2019 Apr;38(17):3170–84.

16. Morgan MJ, Fitzwalter BE, Owens CR, Powers RK, Sottnik JL, Gamez G, et al. Metastatic cells are preferentially vulnerable to lysosomal inhibition. Proc Natl Acad Sci. 2018 Sep 4;115(36):E8479–88.

17. Li S, Song Y, Quach C, Guo H, Jang G-B, Maazi H, et al. Transcriptional regulation of autophagy-lysosomal function in BRAF-driven melanoma progression and chemoresistance. Nat Commun. 2019 Apr 12;10(1):1693.

18. Murrell-Lagnado RD, Frick M. P2X4 and lysosome fusion. Curr Opin Pharmacol. 2019 Aug 1;47:126–32.

19. Jelassi B, Chantôme A, Alcaraz-Pérez F, Baroja-Mazo A, Cayuela ML, Pelegrin P, et al. P2X(7) receptor activation enhances SK3 channels- and cystein cathepsin-dependent cancer cells invasiveness. Oncogene. 2011 May 5;30(18):2108–22.

20. Bolte S, Cordelières FP. A guided tour into subcellular colocalization analysis in light microscopy. J Microsc. 2006;224(3):213–32.

21. Goldman M, Craft B, Brooks A, Zhu J, Haussler D. The UCSC Xena Platform for cancer genomics data visualization and interpretation. bioRxiv. 2018 May 18;326470.

22. Chandrashekar DS, Bashel B, Balasubramanya SAH, Creighton CJ, Ponce-Rodriguez I, Chakravarthi BVSK, et al. UALCAN: A Portal for Facilitating Tumor Subgroup Gene Expression and Survival Analyses. Neoplasia. 2017 Aug 1;19(8):649–58.

23. Burnstock G, Di Virgilio F. Purinergic signalling and cancer. Purinergic Signal. 2013 Dec 1;9(4):491–540.

24. Adinolfi E, Capece M, Amoroso F, De Marchi E, Franceschini A. Emerging Roles of P2X Receptors in Cancer. Curr Med Chem. 2015 Mar 1;22(7):878–90.

25. Di Virgilio F, Ferrari D, Adinolfi E. P2X7: a growth-promoting receptor—implications for cancer. Purinergic Signal. 2009 Jun 1;5(2):251–6.

26. Roger S, Jelassi B, Couillin I, Pelegrin P, Besson P, Jiang L-H. Understanding the roles of the P2X7 receptor in solid tumour progression and therapeutic perspectives. Biochim Biophys Acta. 2015 Oct;1848(10 Pt B):2584–602.

27. Huang P, Zou Y, Zhong XZ, Cao Q, Zhao K, Zhu MX, et al. P2X4 Forms Functional ATP-activated Cation Channels on Lysosomal Membranes Regulated by Luminal pH. J Biol Chem. 2014 Jun 20;289(25):17658–67.

28. Murrell-Lagnado RD. A role for P2X4 receptors in lysosome function. J Gen Physiol. 2018 Feb 5;150(2):185–7.

29. Brisson L, Bański P, Sboarina M, Dethier C, Danhier P, Fontenille M-J, et al. Lactate Dehydrogenase B Controls Lysosome Activity and Autophagy in Cancer. Cancer Cell. 2016 Sep;30(3):418–31.

30. Majora M, Sondenheimer K, Knechten M, Uthe I, Esser C, Schiavi A, et al. HDAC inhibition improves autophagic and lysosomal function to prevent loss of subcutaneous fat in a mouse model of Cockayne syndrome. Sci Transl Med [Internet]. 2018 Aug 29 [cited 2021 Jul 26];10(456). Available from: https://stm.sciencemag.org/content/10/456/eaam7510

31. Westley BR, May FEB. Cathepsin D and breast cancer. Eur J Cancer. 1996 Jan 1;32(1):15–24.

32. Toulme E, Garcia A, Samways D, Egan TM, Carson MJ, Khakh BS. P2X4 receptors in activated C8-B4 cells of cerebellar microglial origin. J Gen Physiol. 2010 Apr 1;135(4):333–53.

33. Cao Q, Zhong XZ, Zou Y, Murrell-Lagnado R, Zhu MX, Dong X-P. Calcium release through P2X4 activates calmodulin to promote endolysosomal membrane fusion. J Cell Biol. 2015 Jun 22;209(6):879–94.

34. Tan S-L, Barri M, Atakpa-Adaji P, Taylor CW, St. John Smith E, Murrell-Lagnado RD. P2X4 Receptors Mediate Ca2+ Release from Lysosomes in Response to Stimulation of P2X7 and H1 Histamine Receptors. Int J Mol Sci. 2021 Jan;22(19):10492.

35. Carnero Corrales MA, Zinken S, Konstantinidis G, Rafehi M, Abdelrahman A, Wu Y-W, et al. Thermal proteome profiling identifies the membrane-bound purinergic receptor P2X4 as a target of the autophagy inhibitor indophagolin. Cell Chem Biol [Internet]. 2021 Mar 15 [cited 2021 Jun 6]; Available from: https://www.sciencedirect.com/science/article/pii/S2451945621001021

36. Izuishi K, Kato K, Ogura T, Kinoshita T, Esumi H. Remarkable Tolerance of Tumor Cells to Nutrient Deprivation: Possible New Biochemical Target for Cancer Therapy. Cancer Res. 2000 Nov 1;60(21):6201–7.

37. Chittaranjan S, Bortnik S, Dragowska WH, Xu J, Abeysundara N, Leung A, et al. Autophagy Inhibition Augments the Anticancer Effects of Epirubicin Treatment in Anthracycline-Sensitive and -Resistant Triple-Negative Breast Cancer. Clin Cancer Res. 2014 Jun 15;20(12):3159–73.

38. Liang DH, Choi DS, Ensor JE, Kaipparettu BA, Bass BL, Chang JC. The autophagy inhibitor chloroquine targets cancer stem cells in triple negative breast cancer by inducing mitochondrial damage and impairing DNA break repair. Cancer Lett. 2016 Jul 1;376(2):249–58.

39. Lazova R, Camp RL, Klump V, Siddiqui SF, Amaravadi RK, Pawelek JM. Punctate LC3B Expression Is a Common Feature of Solid Tumors and Associated with Proliferation, Metastasis, and Poor Outcome. Clin Cancer Res. 2012 Jan 15;18(2):370–9.

40. Mikhaylova O, Stratton Y, Hall D, Kellner E, Ehmer B, Drew AF, et al. VHL-Regulated MiR-204 Suppresses Tumor Growth through Inhibition of LC3B-Mediated Autophagy in Renal Clear Cell Carcinoma. Cancer Cell. 2012 Apr 17;21(4):532–46.

41. Zhitomirsky B, Assaraf YG. Lysosomal accumulation of anticancer drugs triggers lysosomal exocytosis. Oncotarget. 2017 Feb 7;8(28):45117–32.

42. Kundu ST, Grzeskowiak CL, Fradette JJ, Gibson LA, Rodriguez LB, Creighton CJ, et al. TMEM106B drives lung cancer metastasis by inducing TFEB -dependent lysosome synthesis and secretion of cathepsins. Nat Commun. 2018 Jul 16;9(1):2731.

43. Groth-Pedersen L, Aits S, Corcelle-Termeau E, Petersen NHT, Nylandsted J, Jäättelä M. Identification of Cytoskeleton-Associated Proteins Essential for Lysosomal Stability and Survival of Human Cancer Cells. PLOS ONE. 2012 Oct 11;7(10):e45381.

44. Caviston JP, Zajac AL, Tokito M, Holzbaur ELF. Huntingtin coordinates the dynein-mediated dynamic positioning of endosomes and lysosomes. Mol Biol Cell. 2010 Dec 17;22(4):478–92.

45. Biskou O, Casanova V, Hooper KM, Kemp S, Wright GP, Satsangi J, et al. The type III intermediate filament vimentin regulates organelle distribution and modulates autophagy. PLOS ONE. 2019 Jan 30;14(1):e0209665.

46. Cogli L, Progida C, Bramato R, Bucci C. Vimentin phosphorylation and assembly are regulated by the small GTPase Rab7a. Biochim Biophys Acta BBA - Mol Cell Res. 2013 Jun 1;1833(6):1283–93.

47. Ivaska J. Vimentin. Small GTPases. 2011 Jan 1;2(1):51–3.

48. Vuoriluoto K, Haugen H, Kiviluoto S, Mpindi J-P, Nevo J, Gjerdrum C, et al. Vimentin regulates EMT induction by Slug and oncogenic H-Ras and migration by governing Axl expression in breast cancer. Oncogene. 2011 Mar;30(12):1436–48.

49. Mendez MG, Kojima S-I, Goldman RD. Vimentin induces changes in cell shape, motility, and adhesion during the epithelial to mesenchymal transition. FASEB J. 2010;24(6):1838–51.

50. Ketterer S, Mitschke J, Ketscher A, Schlimpert M, Reichardt W, Baeuerle N, et al. Cathepsin D deficiency in mammary epithelium transiently stalls breast cancer by interference with mTORC1 signaling. Nat Commun. 2020 Oct 12;11(1):5133.

51. Miklavc P, Mair N, Wittekindt OH, Haller T, Dietl P, Felder E, et al. Fusion-activated Ca2+ entry via vesicular P2X4 receptors promotes fusion pore opening and exocytotic content release in pneumocytes. Proc Natl Acad Sci. 2011 Aug 30;108(35):14503–8.

Figure 1

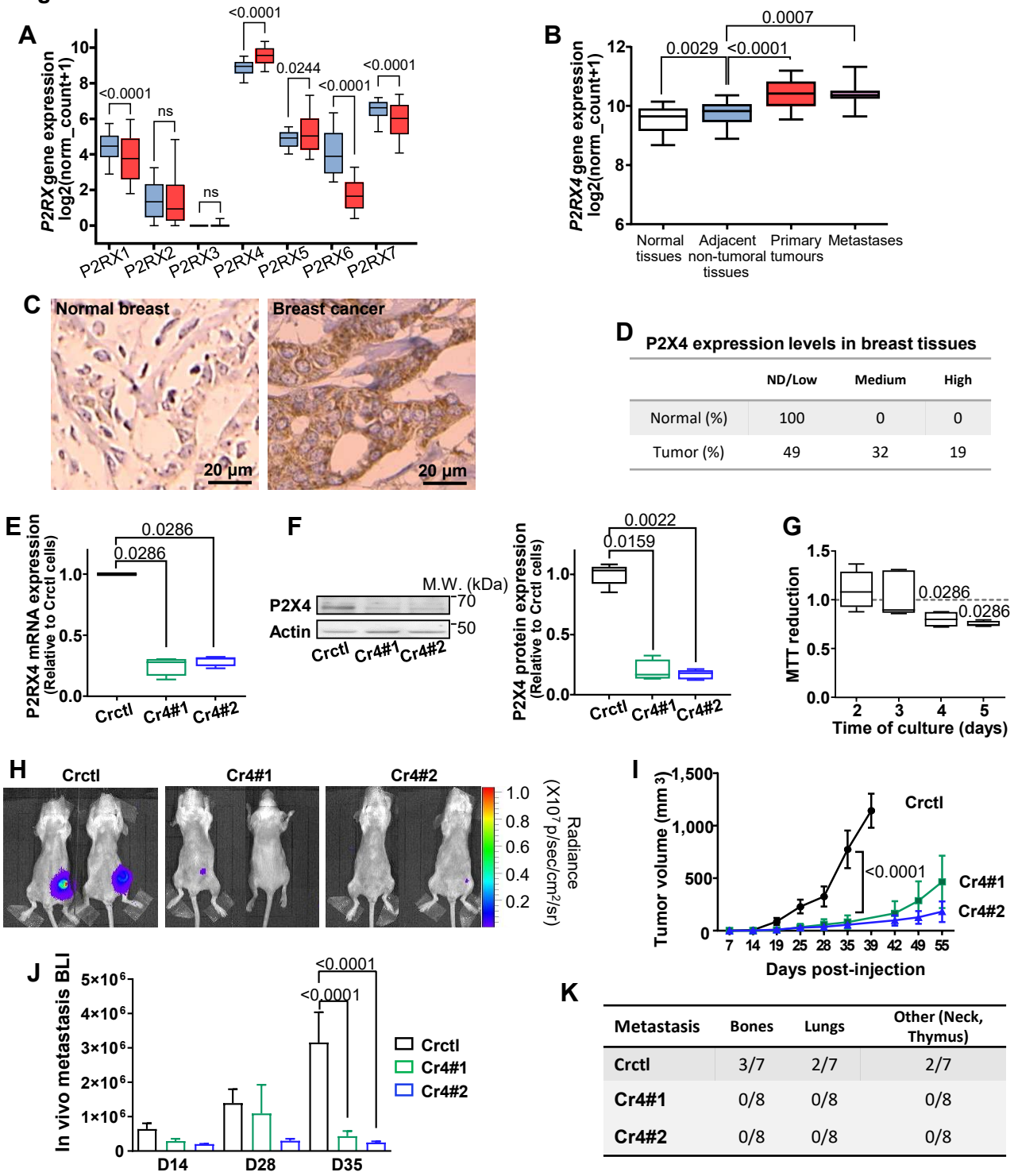

	ND/Low	Medium	High
Normal (%)	100	0	0
Tumor (%)	49	32	19

Metastasis	Bones	Lungs	Other (Neck, Thymus)
Crctl	3/7	2/7	2/7
Cr4#1	0/8	0/8	0/8
Cr4#2	0/8	0/8	0/8

Figure 1. Overexpression of P2X4 is associated with mammary tumour growth and metastatic progression. A, Box plots showing *P2RX1-7* expression in adjacent non-tumoral tissue (blue; n = 114) *versus* primary tumours (red; n = 1,097) in TGCA-BRCA dataset. Expression values were estimated using IlluminaHiSeq and downloaded from UCSC Xena Browser. **B,** Box plots showing *P2RX4* gene expression in normal tissue (n = 179), adjacent non-tumoral tissue (n = 113), primary tumours (n = 1,205) and metastases (n = 7), using the Genotype-Tissue EXpression (GTEx) normal breast and The Cancer Genome Atlas (TCGA) datasets. Expression values were estimated using RSEM norm_count and downloaded from UCSC Xena Browser. **C,** Representative immunohistochemistry staining for P2X4 in normal (10 tissues) and primary breast cancer tissues (108 tissues). Scale bars, 20 µm. **D,** Percentage of tissues with non-detected (ND)/low, medium or high P2X4 staining in breast tissues as in (C). **E,** *P2rx4* mRNA levels, assessed by qPCR, in 4T1 cells transfected with either control CRISPR/Cas9 plasmid (Crctl) or P2X4 CRISPR/Cas9 plasmid (Cr4#1 and Cr4#2). n = 4 independent experiments. **F,** Representative P2X4 protein expression in 4T1 cells transfected as in (E) selected from 4-5 independent experiments. **G,** MTT assay showing Cr4#2 cell viability as a function of time. Data are expressed as fold of Crctl. n = 4-7 independent experiments. **H,** Representative images of bioluminescence in mice at day 28 post-injection. Crctl, Cr4#1 and 2 4T1-luc cells were injected into the mammary fat pad of BALB/c mice. **I,** Tumour volume (in mm^3) was measured with a calliper in the three groups of mice, and is represented as a function of time after cell inoculation. **J,** Bioluminescence imaging (BLI) of metastases was measured in living animals and calculated as the difference between the total BLI and primary tumour BLI in the three groups of mice. **K,** The number and organ distribution of metastases in the three groups of mice. **A, B, E, F, G,** Box plots are shown. Comparisons were performed using the two-tailed Mann–Whitney test. **I, J,** Graphs show the mean ± s.e.m., and the P values were calculated using a Two-way Anova with Tukey's multiple comparison test.

Figure 2

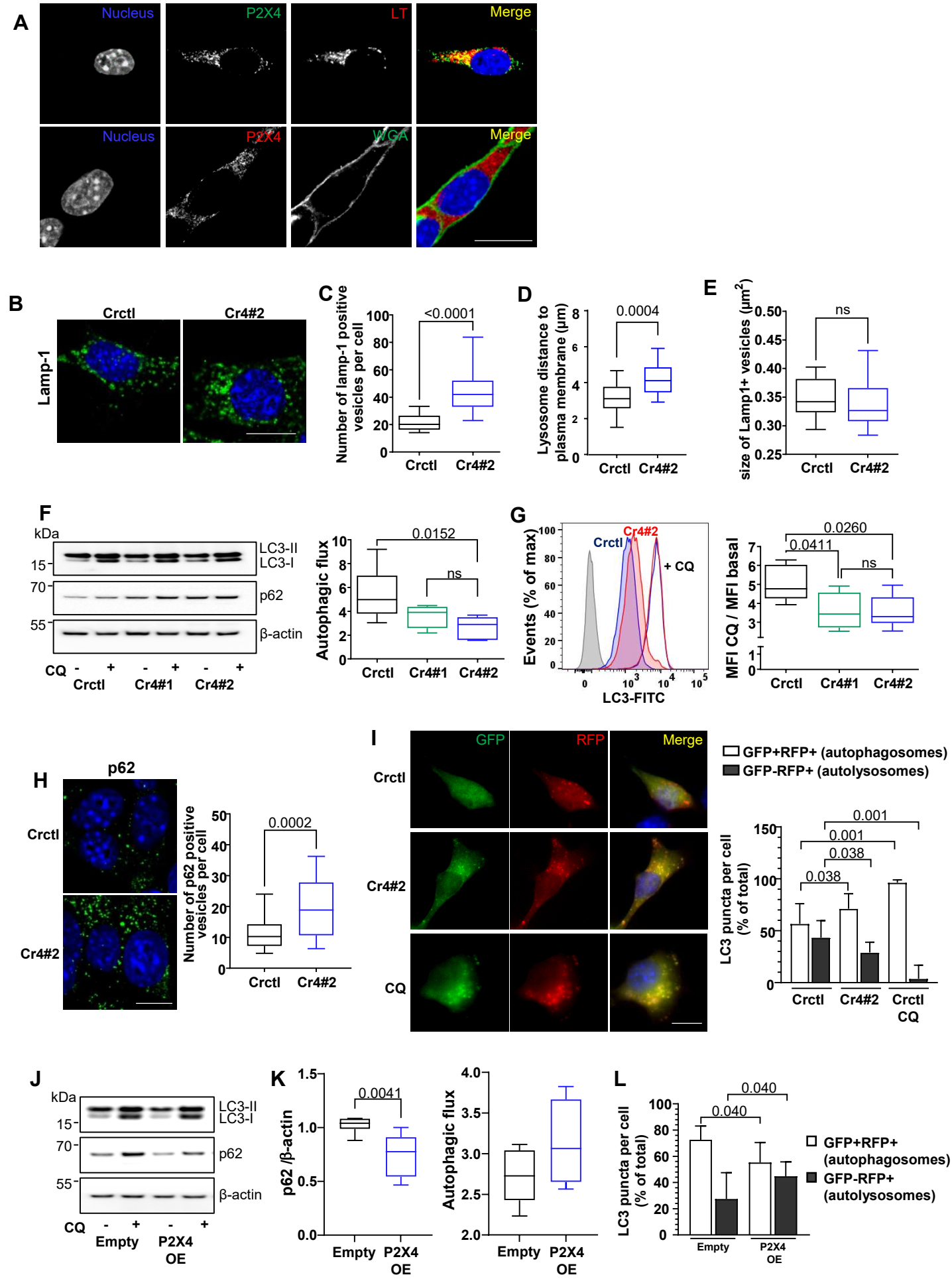
A
Nucleus
P2X4
LT
Merge
Nucleus
P2X4
WGA
Merge
B
Crctl
Cr4#2
Lamp-1
C
Number of lamp-1 positive vesicles per cell
<0.0001
Crctl
Cr4#2
D
Lysosome distance to plasma membrane (µm)
0.0004
Crctl
Cr4#2
E
size of Lamp1+ vesicles (µm²)
ns
Crctl
Cr4#2
F
kDa
15
70
55
LC3-II
LC3-I
p62
β-actin
CQ - + - + - +
Crctl
Cr4#1
Cr4#2
Autophagic flux
0.0152
ns
Crctl
Cr4#1
Cr4#2
G
Events (% of max)
Crctl
Cr4#2
+ CQ
LC3-FITC
MFI CQ / MFI basal
0.0260
0.0411
ns
Crctl
Cr4#1
Cr4#2
H
p62
Crctl
Cr4#2
Number of p62 positive vesicles per cell
0.0002
Crctl
Cr4#2
I
GFP
RFP
Merge
Crctl
Cr4#2
CQ
GFP+RFP+ (autophagosomes)
GFP-RFP+ (autolysosomes)
LC3 puncta per cell (% of total)
0.001
0.001
0.038
0.038
Crctl
Cr4#2
Crctl CQ
J
kDa
15
70
55
LC3-II
LC3-I
p62
β-actin
CQ - + - +
Empty
P2X4 OE
K
p62 /β-actin
0.0041
Empty
P2X4 OE
Autophagic flux
Empty
P2X4 OE
L
LC3 puncta per cell (% of total)
0.040
0.040
Empty
P2X4 OE
GFP+RFP+ (autophagosomes)
GFP-RFP+ (autolysosomes)

Figure 2. P2X4 receptor is partially localised in endolysosomal acidic compartments and controls autophagic flux. A, Representative image of P2X4 immunostaining and co-localization with lysotracker red (LT, top) and WGA (bottom) (Scale bar, 20 µm; n = 3 independent experiments). **B,** Representative confocal images of Lamp-1 immunostaining in Crctl and Cr4#2 4T1 cells (scale bar, 15 µm; from 3 independent experiments). **C,** Quantification of the number of Lamp-1 positive vesicles in 4T1 cells either expressing P2X4 (Crctl) or not (Cr4#2) cultured as in (B) (n = 30-32 images from 3 independent experiments). **D,** Quantification of lysosome distance to plasma membrane in 4T1 cells) cultured as in (B) (n = 24 and 21 cells from 3 independent experiments for Crctl and Cr4#2, respectively.). **E,** Quantification of lysosome size in 4T1 cells) cultured as in (B) (n = 32 images from 3 independent experiments). **F,** LC3-I, LC3-II and p62 expressions analysed by western blot in Crctl, Cr4#1 and Cr4#2 cells either untreated or treated with chloroquine (100 µM) for 6h. Autophagic flux was calculated as the ratio of LC3-II expression with and without chloroquine (n = 4-6 independent experiments). **G,** Representative histogram of LC3-II mean fluorescence intensities in Crctl (blue) and Cr4#2 (Red) cells, untreated or treated with chloroquine, evaluated by flow cytometry (n = 6 independent experiments). **H,** Representative confocal images of p62 immunostaining Crctl and Cr4#2 cells (scale bar, 15 µm; selected from 3 independent experiments) and quantification of the number of p62 positive vesicles in control Crctl and Cr4#2 cells. n = 36 for Crctl and n = 47 for Cr4#2 images from 3 independent experiments. **I,** The proportion of autophagosomes and autolysosomes in 4T1 cells was measured 24 hours after transfection with RFP–GFP–LC3. Cells were treated or not with 100 µM CQ for 4 hours before imaging (scale bar, 15 µm; n = 4). **J,** LC3-I, LC3-II and p62 expressions analysed by western blot in Cr4#2 cells transfected with either empty or P2X4 vector and treated or not with chloroquine (100 µM) for 6h. **K,** Quantification of autophagic flux (n = 6 independent experiments) and p62 protein expressions (n = 7 independent experiments). L, Quantification of autophagosomes and autolysosomes in Cr4#2 cells transfected with either empty or P2X4 vector and cultured as in (I). **C, D, E, F, G, H, I, K,** Box plots are shown. **J, L,** Median with interquartile range are shown. Comparisons were performed using two-tailed Mann–Whitney test.

Figure 3

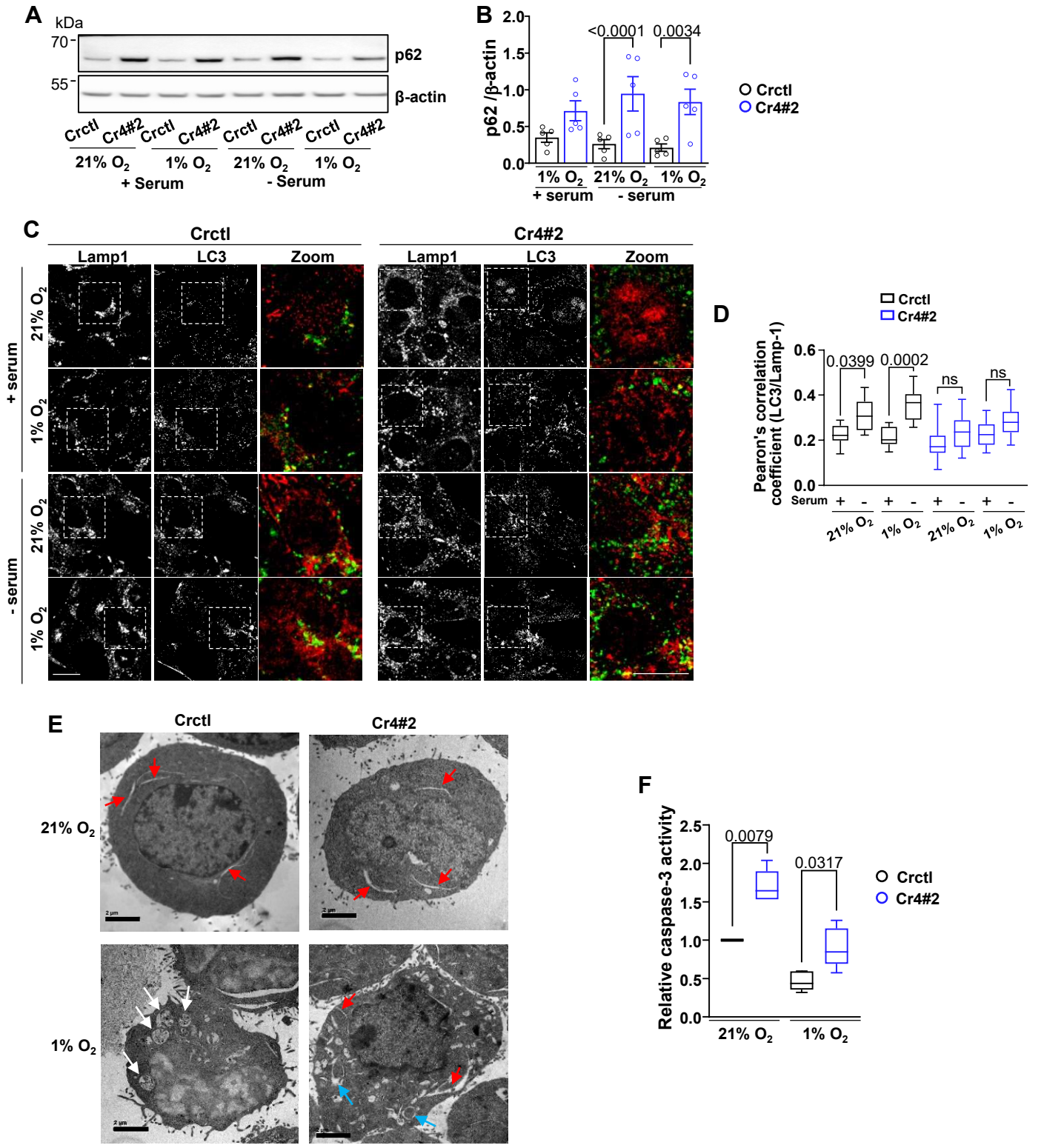

Figure 3. P2X4 receptor regulates autophagy and promotes cancer cell survival under metabolic challenges. A, Representative p62 protein expression in Crctl and Cr4#2 cells cultured for 24h in either 21% or 1% O_2 with or without serum, selected from 5 independent experiments. **B,** Quantification of p62 protein expressions, relative to β-actin (n = 5 independent experiments). **C,** Representative confocal images of Lamp1/LC3 co-staining. Cells were cultured as in (A) and were co-immunostained for Lamp-1 (green) and LC3B (red). **D,** Autolysosome formation was evaluated by calculation of the Pearson correlation coefficient for Lamp-1 and LC3 immunostaining; n represents the number of images analysed. Crctl 21% O_2/+serum, n = 15; Cr4#2 21% O_2/+serum, n = 15; Crctl 1% O_2/+serum, n = 15; Cr4#2 1% O_2/+serum, n = 16; Crctl 21% O_2/-serum, n = 25; Cr4#2 21% O_2/-serum, n = 18; Crctl 1% O_2/-serum, n = 19; Cr4#2 1% O_2/-serum, n = 18, from 3 independent experiments. **E,** Electron microscopy micrographs of autophagic vacuoles in 4T1 cells cultured either in 21% or 1% oxygen for 24h. Red, blue and white arrows indicate phagophores, autophagosomes and autolysosomes, respectively (scale bar, 2 µm; selected from 3 independent experiments). **F,** Caspase-3 activity was evaluated in Crctl and Cr4#2 cells cultured for 24h in either 21% or 1% O_2 with or without serum. The results are normalized to the control condition (Crctl cells cultured under 21% O_2). n = 5 independent experiments. **B,** Graphs show the mean ± s.e.m., and results were compared using a Two-way Anova with Sidak's multiple comparison test. **D, F,** Box plots are shown. Comparisons were performed using Kruskal-Wallis with Dunn's multiple comparisons test and two-tailed Mann–Whitney test, respectively.

Figure 4

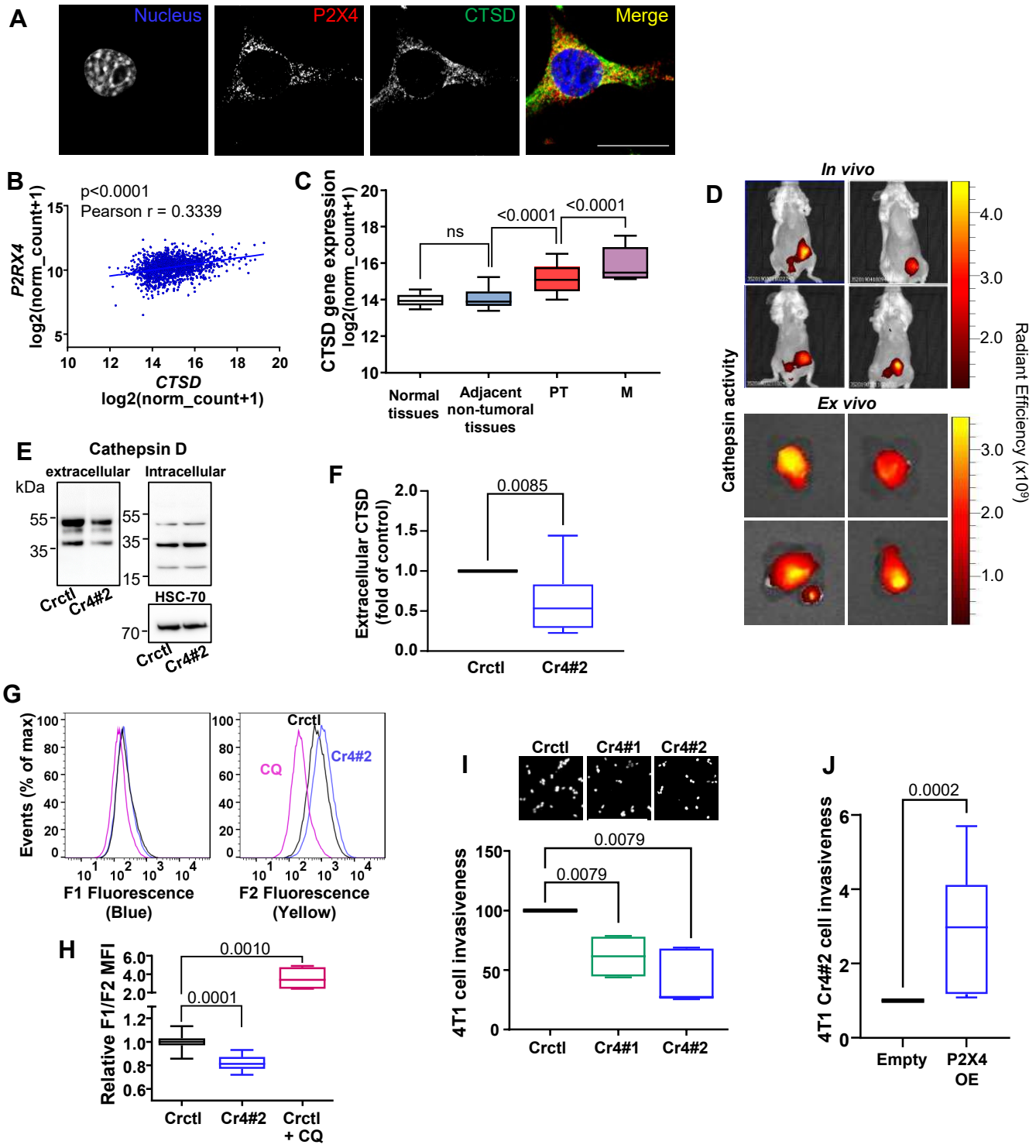

Figure 4. P2X4 receptor regulates lysosomal exocytosis and invasive capacities. A, Representative image of P2X4 immunostaining and co-localization with cathepsin D (CTSD) (Scale bar, 20 µm; n = 3 independent experiments). **B**, Positive correlation between P2RX4 and CTSD genes expression in TGCA target GETEx dataset. Expression values were estimated using RNASeq and analysed as log2(norm_count+1). Shown is the Pearson correlation coefficient (1,391 samples). **C,** Box plots showing CTSD gene expression in normal tissue (n = 179), adjacent non-tumoral tissue (n = 113), primary tumours (n = 1,205) and metastases (n = 7). **D,** Cathepsin activity in vivo and ex vivo. Crctl cells were injected into the mammary fat pad of Balb/cJ mice and cathepsin activity was assessed when tumours reached 100 mm^3 threshold, using ProSense-750 fast probe (n = 4 mice). Mice were images 24h following intravenous probe injection and ex vivo after necropsy. **E,** Cathepsin D protein expression was investigated by western blot intracellularly and extracellularly in 4T1 cells expressing (Crctl) or not (Cr4#2) P2X4. **F,** Quantification of cathepsin D release after 24 h of culture (n = 14 independent experiments). **G,** Flow cytometry analysis of lysosomal pH in Crctl and Cr4#2 4T1 cells, using the ratiometric pH Yellow/Blue LysoSensor dye. Chloroquine (CQ; 100 µM) was used as control for lysosome alkalinisation. **H,** Quantification of the ratio of median fluorescence intensities (Blue/Yellow) in Crctl, and Cr4#2 cells as in (F). n = 10 for Crctl and Cr4#2 conditions. n = 4 for Crctl + CQ condition. **I,** Crctl, Cr4#1 and Cr4#2 cell invasiveness was measured over 24h. Pictures were taken using x10 objective (n = 4-5 independent experiments performed in triplicates). **J,** Invasiveness analysis in Cr4#2 cells transfected with either empty vector or mouse P2X4 vector (n = 8 independent experiments performed in triplicates). Box plots are shown. Comparisons were performed using two-tailed Mann–Whitney test (C, H, I, J) or Wilcoxon matched-pairs signed rank test (F).

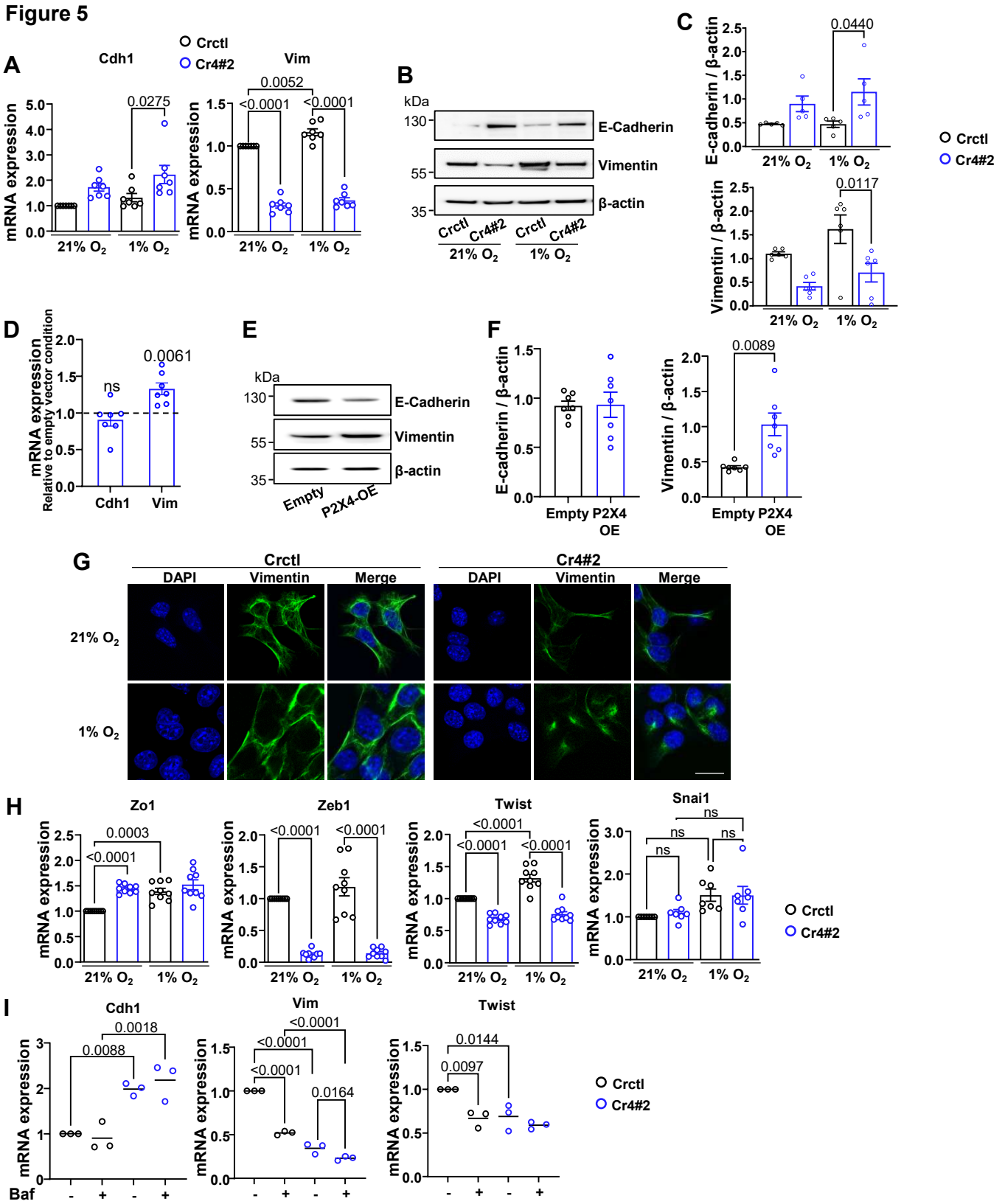

Figure 5. P2X4 drives mammary cancer cells towards a mesenchymal phenotype, associated with increased autophagy. A, mRNA levels of epithelial marker Cdh1 (E-cadherin) and mesenchymal marker Vim (vimentin) in Crctl and Cr4#2 cells cultured in 21% or 1% O_2. Tata Box Protein (Tbp) was used as house-keeping gene. Shown are values and mean from 7 independent experiments performed in triplicates. **B,** E-cadherin and vimentin protein expressions in Crctl and Cr4#2 cells cultured for 24h in either 21% or 1% O_2. **C,** Quantification of E-cadherin (n = 5) and vimentin (n = 6) protein expressions, relative to β-actin, in 4T1 cells as in (B). **D,** mRNA levels of Cdh1 and Vim in Cr4#2 cells transfected with the control vector or P2X4 vector (n = 7 independent experiments performed in triplicates). **E,** E-cadherin and vimentin protein expressions in vector and P2X4 Cr4#2 cells. **F,** Quantification of E-cadherin (n = 7) and vimentin (n = 7) protein expressions, relative to β-actin, in 4T1 cells as in (E). **G,** Confocal imaging of vimentin in Crctl and Cr4#2 4T1 cells. Representative pictures from 3 independent experiments. **H,** mRNA levels of epithelial marker Zo1, and mesenchymal transcription factors Twist, Snai1 and Zeb1, in Crctl and Cr4#2 cells cultured in 21% or 1% O_2. Shown are values and mean from 7-9 independent experiments performed in triplicates. **I,** mRNA levels of Cdh1, Vim and Twist in Crctl and Cr4#2 4T1 cells cultured during 24h with or without 100 nM of bafilomycin A1 (Baf). Shown are values and mean from 3 independent experiments performed in triplicates. Graphs show the individual values and the mean ± s.e.m., and results were compared using a one-way Anova with Tukey's multiple comparison test (**A, C, H, I**) or Student's t test with Welch's correction (**D, F**).